https://doi.org/10.5194/egusphere-2023-2015
Preprint. Discussion started: 26 September 2023

Real-time Monitoring and Analysis of Debris Flow Events: Insight from seismic signal features and dynamic flow characteristics

Yan Yan[a,c], Cheng Zeng[a], Yifei Cui[b]*, Sheng Hu[d], Xinglu Wang[a], Hui Tang[e]

[a] Key Laboratory of High-Speed Railway Engineering, MOE/School of Civil Engineering, Southwest Jiaotong University, Chengdu 610031, China

[b] State Key Laboratory of Hydroscience and Engineering, Tsinghua University, Beijing 100084, China

[c] Section 4.6: Geomorphology, German Research Centre for Geosciences (GFZ), Potsdam 14473, Germany

[d] College of Urban and Environmental Sciences, Northwest University, Xi'an 710127, China

[e] Section 4.7: Earth Surface Process Modelling, German Research Centre for Geosciences (GFZ), Potsdam 14473, Germany

*Corresponding author: Yifei Cui, e-mail: yifeicui@mail.tsinghua.edu.cn

https://doi.org/10.5194/egusphere-2023-2015
Preprint. Discussion started: 26 September 2023

Abstract

Debris flows are among the most dangerous natural hazards worldwide because they start abruptly, move quickly, and transport large boulders, causing great loss of life and infrastructure. The most important approach to preventing and mitigating debris flows is through monitoring and early warning. In recent years, environmental seismology has emerged as a powerful method for monitoring debris flows because it allows non-contact observation over large areas and can provide extensive information on debris flow dynamics. However, further research is required on combining debris flow imagery with seismic signal analysis, incorporating information from post-disaster surveys, and the inversion of seismic signals into dynamic parameters of debris flows. Here, we aim to explore the basic parameters, development process, and magnitude of debris flows based on seismic signal analysis combined with other information recorded in real time during the formation and development of three debris flows in Wenchuan, China. The analysis involves three stages. First, we compensate for the energy loss of the seismic signal due to the absorption attenuation effect and restore the signal to an unchanged state as far as possible. Second, we identify the start and end time of the debris flow from the seismic signal, analyze the rainfall data to determine that the debris flow was triggered by the test rain, and determine that changes in the energy and frequency ranges of the seismic signal are highly consistent with the development of the debris flow. Third, a comprehensive analysis of debris flow images, the power spectral density (PSD) of the seismic signal, and forward modeling of the PSD of the seismic signal of the debris flow are used to reveal the relationship between the seismic signal and the development process of the debris flow and clarify the feasibility of debris flow analysis from the time-frequency characteristics of the seismic signal. Debris flow exhibits the characteristics of fast excitation and slow recession. Using the cross-correlation algorithm and verifying Manning's formula, a maximum velocity of 7.027 m/s was calculated for the second debris flow. A comparison of the

https://doi.org/10.5194/egusphere-2023-2015
Preprint. Discussion started: 26 September 2023

frequency characteristics of the seismic signal allowed the relative magnitude of the three debris flows to be assessed. The study provides a theoretical basis and a case study exemplar for the reconstruction of the debris flow process and peak velocity estimation using debris flow seismology, offering a framework for upscaling debris flow monitoring networks and the determination of early warning thresholds.

Keywords: Seismic wave; debris flow; monitoring; kinematic characteristics; Wenchuan (China)

1 Introduction

Debris flows comprise a solid-fluid mixture that, under heavy rainfall (Iverson, 1997), can generate huge surges that cause damage and loss of life. There are many recent examples worldwide, including a large-scale debris flow in Zhouqu County, Gansu Province, China, on August 7, 2010, that killed 1,765 people and damaged more than 5,500 houses (Tang et al., 2011) and one in Montecito, California, USA on January 9, 2018, that resulted in 189 casualties and damage to 408 houses (Kean et al., 2019). Due to the high hazard potential of debris flows, there is great interest in disaster reduction measures, with monitoring and early warning systems the most widely used at present. On-site monitoring provides information on the nature and characteristics of debris flow, and monitoring of rainfall, flow velocity, and flow depth can feed into early warning systems for disaster reduction (Tecca et al., 2003; Suwa et al., 2009; Hürlimann et al., 2019).

Existing systems for debris flow monitoring and early warning focus on factors contributing to their triggering, formation, and evolution (Arattano and Marchi, 2008). The main triggering element studied is rainfall, and early warning thresholds are based on different aspects of rainfall intensity or duration (Chien-Yuan et al., 2005; Chen et al., 2007; Hürlimann et al., 2014, 2019; Cui et al., 2018; Liu et al., 2021). Hürlimann et al. (2014) suggested a combination of average rainfall intensity and duration is best for defining a rainfall threshold or critical value. Cui et al. (2018) proposed a method for

https://doi.org/10.5194/egusphere-2023-2015
Preprint. Discussion started: 26 September 2023

distinguishing debris flows from flood events based on the relationship between rainfall intensity and duration. However, reliance on historical rather than real-time rainfall data makes it difficult to determine the rainfall threshold, and the transferability of rainfall-based monitoring and early warning is poor.

Alternative approaches to monitoring and early warning based on debris flow formation and evolution use flow velocity and flow depth as the main indicators (Arattano and Moia, 1999; Marchi et al., 2002; Kogelnig et al., 2014; Hürlimann et al., 2019). Flow depth and velocity are usually combined with monitoring section geometry to estimate discharge and analyze evolutionary characteristics (Arattano and Marchi, 2008; Hürlimann et al., 2019). A key advantage of this approach is that the early warning threshold (e.g., debris flow occurrence) can be easily determined (Arattano and Marchi, 2008). Based on monitoring debris flows in Acquabona Creek in the Italian Alps, Berti et al. (2000) highlighted how hydrological characteristics changed over time, with higher solid phase concentration and lower velocity (4 m/s) in the initial surge. In a study of a channel at Illgraben in the Swiss Alps, Hürlimann et al. (2003) showed three debris flows had different properties, such as flow depth, flow velocity, and peak flow. Monitoring and early warning systems based on debris flow initiation and evolution must identify potential sites in advance so that suitable instrumentation can be installed. However, the abruptness of onset and high strength of the initial debris flow surge often damage close-range monitoring instruments making it difficult to obtain a complete dataset of the entire debris flow process. This poses a huge challenge to the monitoring and early warning of debris flows.

New monitoring methods are urgently needed to improve debris flow monitoring, and in the last decade or so, the development of environmental seismology has offered a new approach (Hibert et al., 2011; Moretti et al. al., 2012; Ekström and Stark, 2013; Barrière et al., 2015; Dammeier et al., 2016; Cook and Dietze, 2022). Environmental seismology has been applied to monitor landslides (Li et al., 2017; Fuchs et al., 2018), rockfalls (Deparis et al., 2008; Vilajosana et al., 2008), avalanches (Schneider et al.,

https://doi.org/10.5194/egusphere-2023-2015
Preprint. Discussion started: 26 September 2023

2010; Van Herwijnen and Schweizer, 2011), as well as debris flow (Arattano, 1999; Burtin et al., 2009; Schimmel and Hübl, 2016; Walter et al., 2017; Lai et al., 2018). The main advantages of the approach are long-distance, non-contact monitoring and rich information on event dynamics (Arattano and Marchi, 2008; Hübl et al., 2013; Kogelnig et al., 2014; Marchetti et al., 2019). For debris flows, seismic monitoring can record details of the evolution of an event, which is crucial for analyzing movement characteristics and providing an appropriate warning. Using the amplitude source location method, Walter et al. (2017) detected a debris flow event half an hour before it reached the gully mouth. Lai et al. (2018) proposed a new physical debris flow model that allows flow velocity and distance to be calculated based on the amplitude and frequency characteristics of the seismic signal. Andrade et al. (2022) proposed a simple positive linear relationship between the peak amplitude of the seismic signal and the peak flow rate of the debris flow. Current research on seismic monitoring and debris flow early warning concentrates on event timing (Walter et al., 2017; Huang et al., 2020; Beason et al., 2021), location (Walter et al., 2017; Lai et al. al., 2018), evolution of parameters such as velocity and flow (Arattano, 1999; Lai et al., 2018; Andrade et al. 2022; Schimmel et al., 2022), and identification (Bessason et al., 2007; Schimmel and Hübl, 2016; Huang et al., 2020). To enable the widespread adoption of debris flow early warning systems using seismic monitoring, the approach needs to be standardized, quantified, and systematized (Bessason et al., 2007; Arattano et al., 2015; Allstadt et al., 2019). However, this is constrained at present by a lack of detail in understanding the characteristics of the debris flow seismic signal and the debris flow evolution process.

This study investigates the time-frequency domain characteristics of the seismic signal during debris flow evolution based on real-time field monitoring of three debris flows on August 19, 2022, in the Wenchuan Earthquake area of China. Based on in-gully monitoring systems comprising seismic equipment, rainfall gauge, and infrared camera, seismic signal processing, and quantitative analysis are combined with real-time rainfall data and infrared monitoring. Analysis of debris flow kinematic

https://doi.org/10.5194/egusphere-2023-2015
Preprint. Discussion started: 26 September 2023

characteristics provides a theoretical basis for reconstruction and inversion of the debris flow process. The study offers a framework for establishing a debris flow identification, monitoring, and early warning system.

2 Study site and field monitoring system

2.1 Study area

The study area, in Wenchuan County, Sichuan Province, China (Figure 1), is characterized by north-northeast trending mountains, divided by the Minjiang River and its tributaries. The area is typical of that formed by tectonic uplift and river erosion, with undulating terrain, ravines, and steep gradients. River channel gradients range from 5° to 30°, hillslopes range from 25° to 50°, and most of the area has a humid climate (Guo et al., 2016). Seismic activity is frequent, and much of the landscape still shows signs of the Wenchuan Earthquake of May 12, 2008, with widespread loose rocks and soils that provide ample sediment sources for debris flow. This study focuses on Ergou and Fotangbagou gullies in the Minjiang River Basin. The watersheds have experienced many debris flows in recent years, threatening nearby villages, road transportation, and hydropower stations.

https://doi.org/10.5194/egusphere-2023-2015
Preprint. Discussion started: 26 September 2023

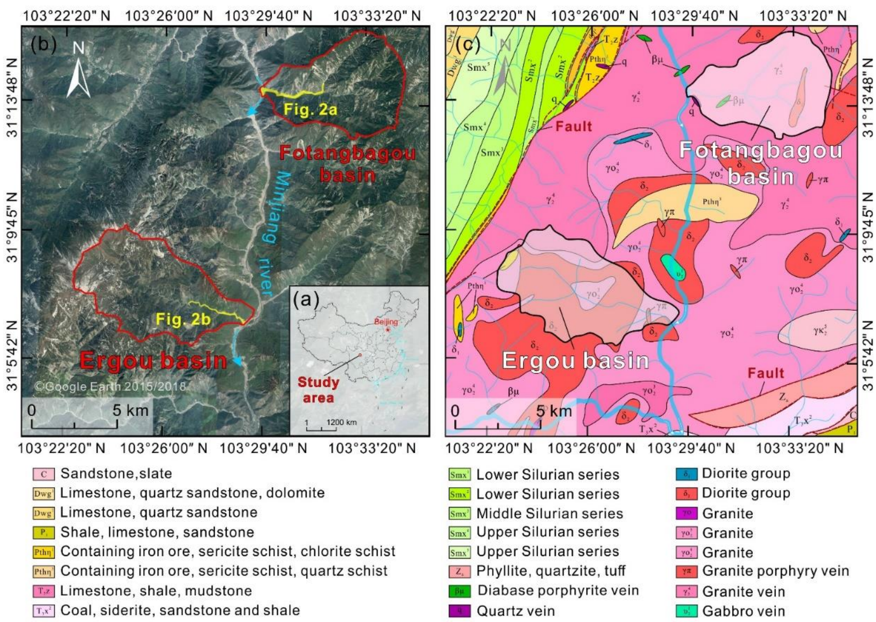

Figure 1. Overview of the study area. (a) Location of the study area within China; (b) The two study catchments, Ergou and Fotangbagou, on the Minjiang River, Wenchuan, Sichuan, China. The background image is from ©Google Earth 2015/2018; (c) Regional geology, the original vector data is from China National Digital Geological Map (Public Version at 1：200 000 Scale) Spatial Database (Li et al., 2019).

Ergou gully drains an area of 39.4 km^2 and is about 6 km from the epicenter of the Wenchuan Earthquake; it ranges in altitude from 930 to 4120 m, has a channel length of about 12 km, the average slope of about 12°, and a debris flow circulation area of between 5 to 12° (Guo et al., 2016). The gully is located on the right bank of the Minjiang River and drains west to east, with steep walls, abundant water sources, and a narrow and winding channel. The average slope is 18.45%. Important nearby infrastructure at risk includes a factory at the end of the gully, a village on the left bank of the Minjiang River facing the gully mouth, and national highway G213 adjacent to the bank.

The Fotangbagou gully basin has an area of 33.6 km^2; it ranges in altitude from

https://doi.org/10.5194/egusphere-2023-2015
Preprint. Discussion started: 26 September 2023

1117–3462 m, has a channel length of about 9.78 km, and has bank slopes of 25–45° (Cao et al., 2019). The gully is on the left bank of the Minjiang River and drains east to west. The gully has adequate water sources, with steep walls and a wide and gently winding channel. The average slope ratio is 10.71%. There are hydropower stations on the Minjiang River near the gully and on the north side of the gully mouth.

2.2 Monitoring systems

Monitoring systems comprising an array of instruments were set up at upstream (station 1) and downstream (station 2) monitoring points in Fotangbagou and Ergou gullies (Table 1, Figure 2), in 2022 and 2021 respectively. The distance along the river course between the two monitoring points in Fotangbagou Gully is about 520 m and about 460 m in Ergou Gully. In Fotangbagou Gully, seismographs from Chengdu Baixinyuan Science Technology Company Limited were used for seismic monitoring; these incorporate velocity sensors, acceleration sensors, etc., with a sampling frequency of 100 Hz. In Ergou Gully, seismic signal monitoring (Geophone) and acquisition (Data-Cube) equipment, provided by the Helmholtz Potsdam Center and German Geoscience Center, was used with a sampling frequency of 100 Hz and an eigenfrequency of 4.5–150 Hz. Rain gauges were installed near the upstream monitoring points (3260 m from the mouth in Fotangbagou Gully and 4130 m in Ergou Gully) to record rainfall in the channel. Each observation station was also equipped with an infrared camera to record the debris flow at 5-minute intervals in real time to provide particle size data and other data to verify the seismic reconstruction. The cameras have several tens of meters of visibility at 2592×1944 dpi resolution in the daytime and about 2 to 4 m visibility at 1920×1080 dpi resolution at night.

https://doi.org/10.5194/egusphere-2023-2015
Preprint. Discussion started: 26 September 2023

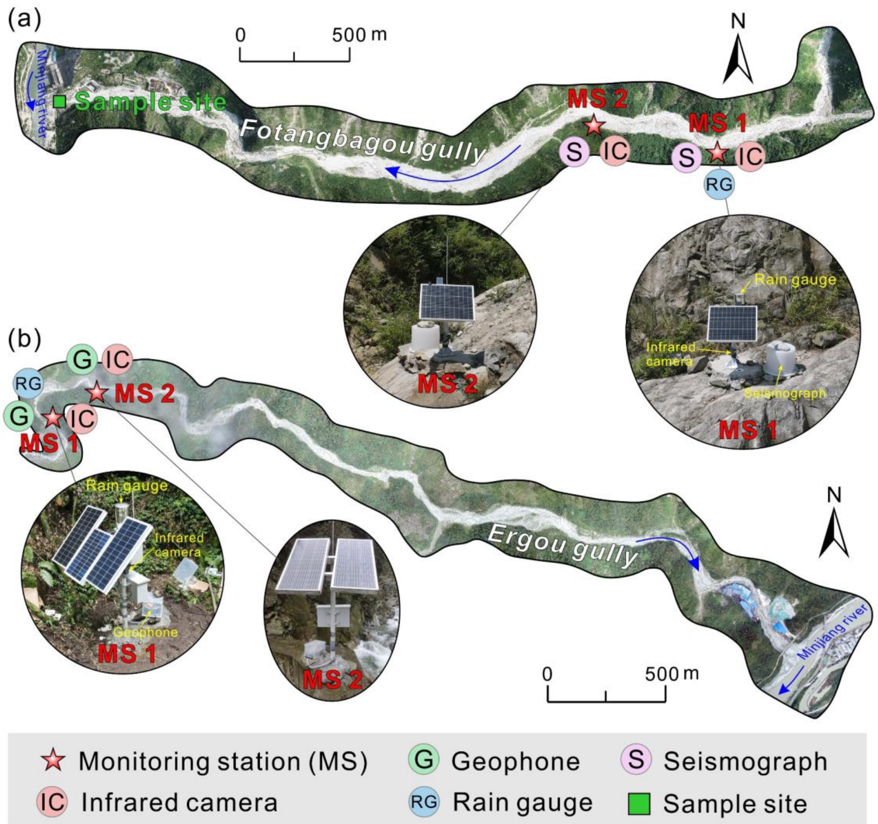

Figure 2. Schematic overview of monitoring network layout in the two study catchments. (a) Fotangbagou gully; (b) Ergou gully. See Figure 1 for gully locations.

Table 1 Instrument parameters for monitoring stations in the two study catchments.

Equipment	Instrument parameters	
	Fotangbagou gully	Ergou gully
Seismograph	Sampling rate 100 Hz	—
Geophone	—	Sampling rate 100 Hz
Rain gauge	Record once per hour with a resolution of 0.2 mm	
Infrared camera	1 shot every 5 minutes at 2592×1944, 1920×1080 dpi resolution during the day and at night	

3 Methodology

To extract information on debris flow evolution, seismic signals were processed

https://doi.org/10.5194/egusphere-2023-2015
Preprint. Discussion started: 26 September 2023

following the procedure in Figure 3. The key steps are outlined below.

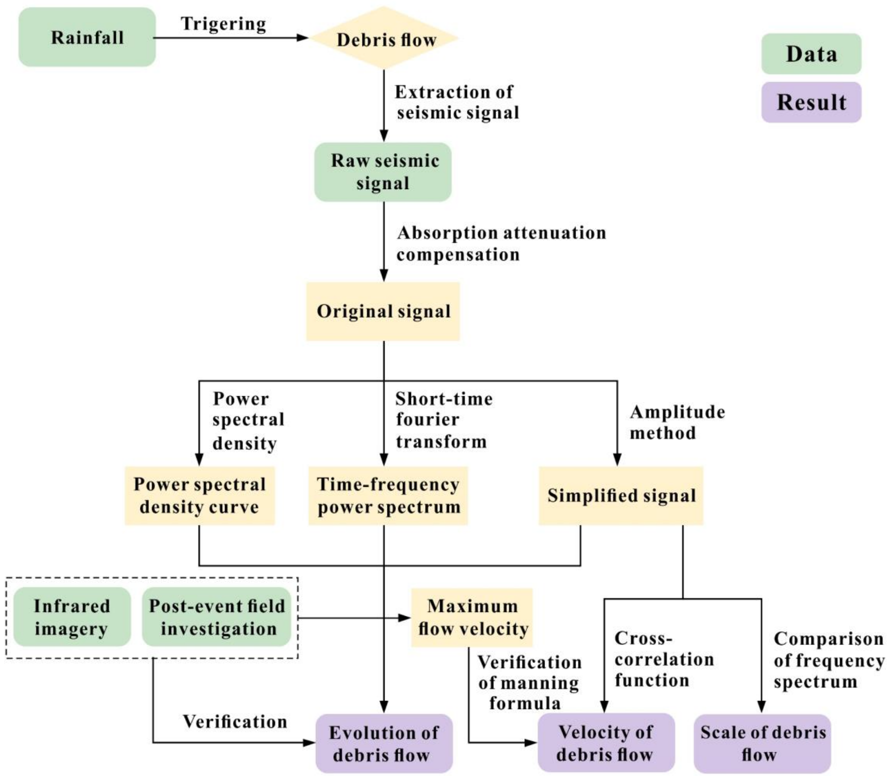

Figure 3. Research methodology for processing and analysis of debris flow seismic signal.

3.1 Short-time Fourier transform

The short-time Fourier transform (STFT, Equation (1)) is used to analyze the time-frequency domain characteristics of the debris flow seismic signal (Yan et al., 2021, 2022, 2023). The method allows the time domain and frequency domain characteristics of the signal to be analyzed simultaneously:

$$X(n,\omega)=\sum_{m=-\infty}^{\infty}x(m)\omega(n-m)e^{-j\omega m}, \tag{1}$$

where m is the window start time, ω is the angular frequency, e is a natural constant, n is the time series, and j is the imaginary number (Yan et al., 2021). A Hanning window

https://doi.org/10.5194/egusphere-2023-2015
Preprint. Discussion started: 26 September 2023

length of 2056 is used.

3.2 Cross-correlation function

Since the same signal propagates to many places, there is a time difference τ between receipt of the signal at different sampling locations, such as M signal samples $[x_K]$, $[y_K]$ in Equations (2) and (3). The cross-correlation algorithm is used to solve the signal time delay of the same signal at different locations when the maximum calculation result $\phi_{yx}(\tau)$ is obtained based on Equation (4) (Arattano and Marchi, 2005; Comiti et al., 2014). In the context of debris flows, the average flow velocity between monitoring stations can be obtained by dividing the distance between the stations by the signal time delay. This method has been used to objectively calculate the average velocity of debris flows (Coviello et al., 2015):

$$[x_K] = [x_0, x_1, x_2, \ldots, x_{M-1}] \quad (2)$$

$$[y_K] = [y_0, y_1, y_2, \ldots, y_{M-1}] \quad (3)$$

$$\phi_{yx}(\tau) = \sum_{t=0}^{M-1} x_t y_{t+\tau} \, , \quad (4)$$

where t and K are from 0 to M-1.

3.3 Manning formula calculation

The Manning formula (Equation 5) is used to calculate the peak flow velocity of a debris flow passing through a section based on characteristic terrain parameters of the section (Yu and Lim, 2003; Cui et al., 2013; Guo et al., 2016). Here, the velocity calculated using the Manning formula is compared with that from the cross-correlation method, to verify the relative accuracy of the cross-correlation algorithm:

$$v = \frac{1}{n} J^{\frac{1}{2}} R^{\frac{2}{3}} \, , \quad (5)$$

where v represents debris flow velocity, n represents the roughness coefficient of the channel, J is the slope ratio of the section, and R is the hydraulic radius of the section.

In Equation (5), n is calculated using Equation (6) (Smart, 1999):

https://doi.org/10.5194/egusphere-2023-2015
Preprint. Discussion started: 26 September 2023

$$n = \frac{d_{50}^{\frac{1}{6}}}{6.7\sqrt{g}}, \quad (6)$$

where d_{50} represents the median particle size, and g represents the acceleration due to gravity.

3.4 Power spectral density

Power spectral density (PSD, Equation (7)) can be used to estimate power per frequency for different frequencies in a specific period (Yan et al., 2020), and allows debris flow evolution to be analyzed from the seismic signal.

$$PSD_{f_{\min}\sim f_{\max}}(t) = \frac{1}{(f_{\max} - f_{\min})} \times \sum_{f=f_{\min}}^{f_{\max}} S(t, f)df, \quad (7)$$

where $f_{\min}$ and $f_{\max}$ represent minimum frequency and maximum frequency, respectively, t is time for the seismic signal, and $S(t, f)$ represents the time-frequency power spectrum base on STFT (Yan et al., 2017).

PSD can be calculated by Equation (8) based on seismic signals (Lai et al., 2018).

$$PSD \approx 1.9 \cdot LWD^3 u^3 \cdot \frac{f^{3+5\xi}}{v_c^5 r_0} e^{-\frac{8.8 f^{1+\xi} r_0}{v_c Q}}, \quad (8)$$

where L is effective length, W is width of the channel, D represents the 94th centile of the grain size distribution, u represents debris flow velocity, f is frequency, v_c is Rayleigh wave phase velocity at 1 Hz, r_0 is distance between the monitoring station and channel, ξ=0.4 is a parameter related to how strongly seismic velocities increase with depth at the site, and Q is an attenuation factor (Tsai et al., 2012; Lai et al., 2018).

3.5 Absorption attenuation compensation

Elastic wave travel through the earth is energy dissipation and velocity dispersion, the two effects are a function of frequency and mathematically expressed by Equation 9 with some parameters (Kjartansson,1979; Futterman, 1962; Strick,1967). It can be used to restore a part of energy loss as:

$$h(t, f) = e^{-\frac{\pi f t}{Q}\left|\frac{\omega_0}{\omega}\right|^{\frac{2}{\pi}\arctan\left(\frac{1}{2Q}\right)}}, \quad (9)$$

https://doi.org/10.5194/egusphere-2023-2015
Preprint. Discussion started: 26 September 2023

where f is the frequency of the seismic signal, t is the spreading time, Q represents Quality Factor quantitatively depicting the absorption attenuation, and ω_0 and ω are reference angular velocity at 1 Hz (ω_0=2π) and angular velocities, respectively. When the amplitude at a certain frequency has decayed greater, a compensation function (Equation 10) can be used to restore the part of the signal decaying at that frequency range (Liu et al., 2013):

$$\Gamma(t, f) = \frac{h(t, f) + \sigma^2}{h^2(t, f) + \sigma^2}, \tag{10}$$

where σ is a constant, with a σ^2 value of 0.02 used here.

4 Results and analysis

4.1 Seismic data and rainfall monitoring

The debris flow monitoring system recorded seismic signals with a high signal-to-noise ratio for all three debris flow events (Figure 4). In each event, seismic amplitude rises rapidly and decreases gradually, and seismic signals are high frequency with wide frequency bands (Figures 4a, 4c), but the frequency bands differ (Figures 4b, 4d). The first and second debris flows in the Fotangbagou gully have frequency bands of 10–40 Hz and 5–45 Hz, and the Ergou gully debris flow has 5–45 Hz. By analyzing the amplitude and time-frequency spectrum variation, we can roughly get the starting and ending times of each event (Table 2).

Table 2 Starting and ending time of three debris flow events at Wenchuan, China (August 19, 2022), picked from the seismic signals.

	Fotangbagou		Ergou
	1st	2nd	
Starting	3:00 am	7:30 am	2:00 am
Ending	4:30 am	11:00 am	5:00 am

https://doi.org/10.5194/egusphere-2023-2015
Preprint. Discussion started: 26 September 2023

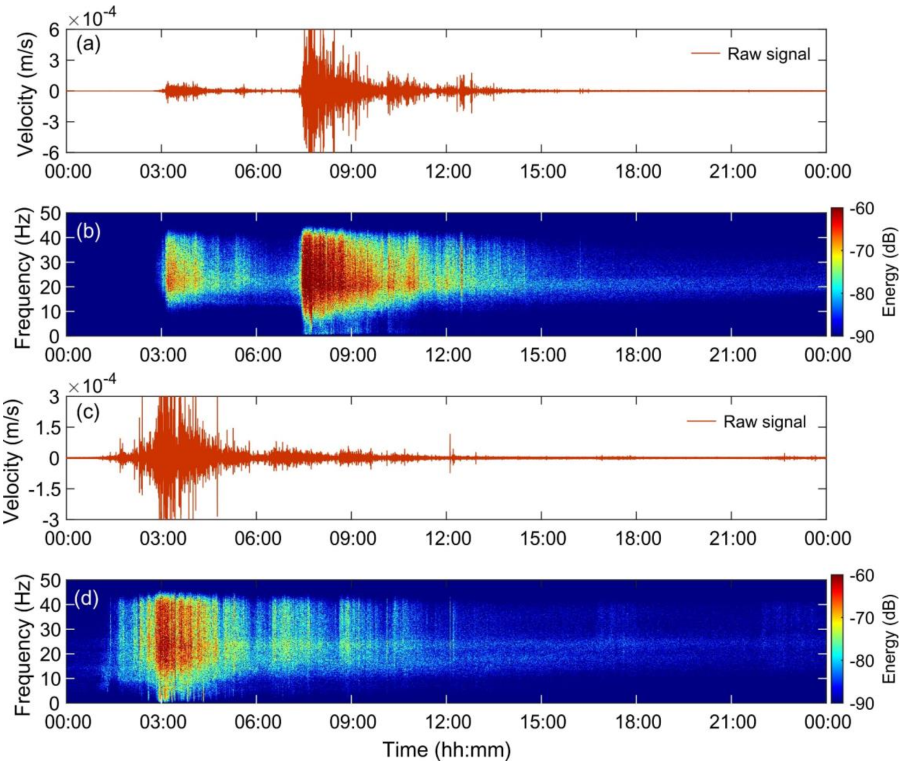

Figure 4. Vertical seismic and frequency spectrum of the debris flows. (a) Raw seismic from the 2nd Fotangbagou gully debris flow at station 1; (b) time-frequency spectra of (a) by STFT; (c) Raw seismic from Ergou gully at station 2; (d) time-frequency spectra of (c).

The rainfall record for Fotangbagou Gully shows hourly rainfall of 6.4 mm and 14.2 mm before the starting time of the first and second debris flows, respectively, and daily cumulative rainfall totals of 15.6 mm and 30.2 mm (Figure 5a). In Ergou Gully, the hourly rainfall before the debris flow outbreak is 3.8 mm, and cumulative rainfall is 10.8 mm (Figure 5b). The rainfall data analysis reveals that there is a large intensity of precipitation before the eruption of three debris flows and the rainfall data coupling with the key time identified by seismic signals. Initiation of the two debris flows in Fotangbagou Gully coincided with hourly rainfall maxima (second highest and highest) of the 24 h period, but the Ergou Gully debris flow did not correspond with an hourly rainfall maximum. However, cumulative rainfall before the initiation of the Ergou debris flow reached 15 mm, which was greater than the cumulative rainfall of the first debris flow event in the Fotangbagou gully. Thus, rainfall is regarded as the triggering factor for debris flow initiation in the two gullies.

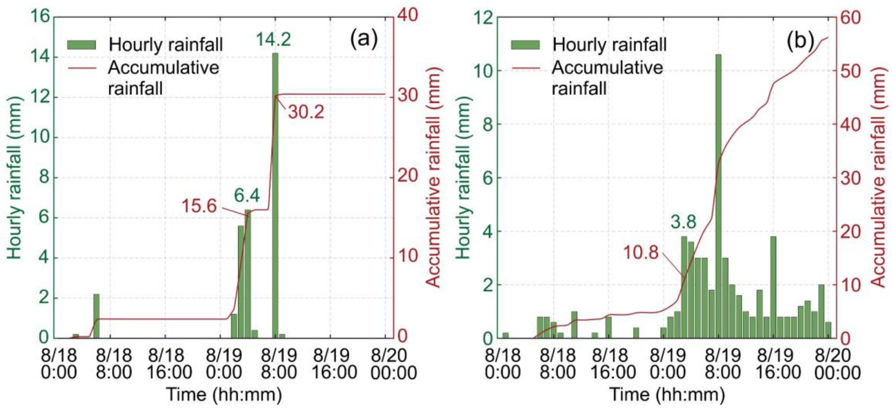

Figure 5. Hourly and cumulative rainfall at the two study sites from August 18 to 19, 2022 (UTC+8). (a) Fotangbagou gully; (b) Ergou gully.

Plane waves propagating through subsurface earth are energy dissipation along with frequency and velocity dispersion. We use Equations (9) and (10) to compensate for a certain extent of loss to exquisite relatively original seismic triggered by debris flow. The entire debris flow through the channel will generate ground vibration and spread to the monitoring site. Therefore, the signal recorded by the site is a superposition of the vibration that the entire debris flow stimulates to spread to the site at this frame, which indicates the debris flow signal has characteristics of a "line source". During the seismic signal compensation, it is difficult for us to determine the travel time of the debris flow signal. River channels are about 10 m around the site during the processing signal. The average distance between the river channel and the site is calculated, and we use this value to calculate the average travel time t of the seismic signals. The horizontal distances between the channel and monitoring points 1 and 2

https://doi.org/10.5194/egusphere-2023-2015
Preprint. Discussion started: 26 September 2023

are 15 m and 25 m for the Fotangbagou gully. The dataset for the second Fotangbagou debris flow is the most complete, so the seismic signal for that event was restored first (Figure 6). For monitoring points 1 and 2, we use Q factors of 4 and 2.4, Rayleigh wave velocities of 800 m/s and 500 m/s at 1 Hz, and seismic travel time of 0.02 s and 0.04 s. The gain limit of the two sites σ^2=0.02. From the compensation spectrum curve, the high-frequency component has been greatly restored, and the spectrum curve of the two sites is similarly improved; from the time domain curve, the characteristics change of the curve after the compensation of site two further improved the similarity of site one, and its characteristics change is more obvious. From the perspective of effect, the compensation effect is relatively good, and the effect of the absorption attenuation on the debris flow seismic signal can be weakened to a certain extent. Thus, we will use the compensated relative original seismic for further analysis in the next sections.

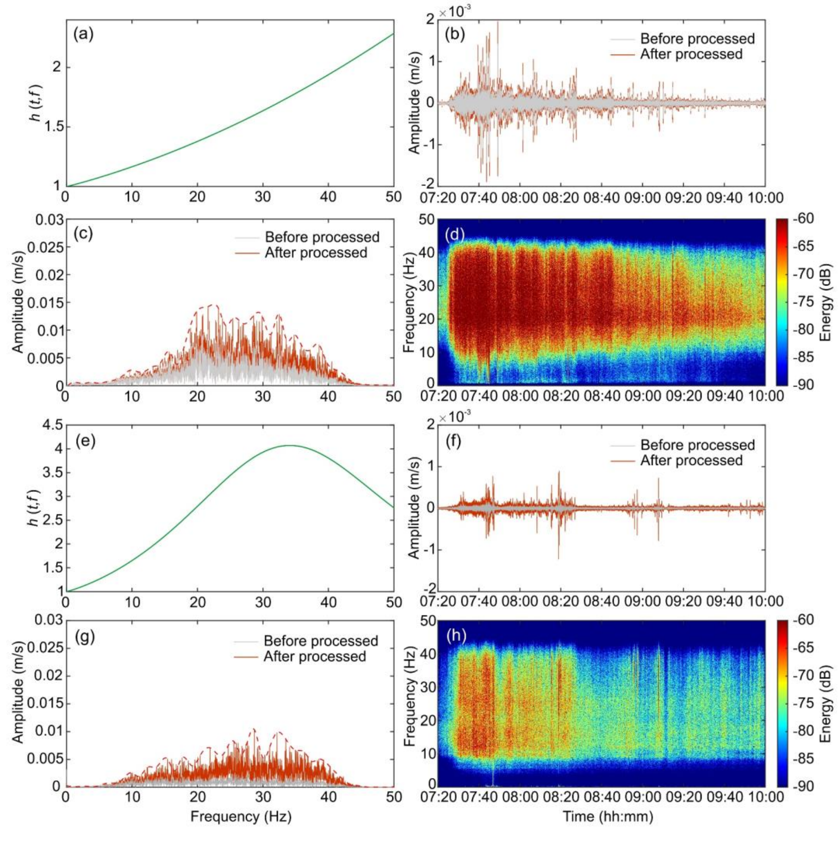

https://doi.org/10.5194/egusphere-2023-2015
Preprint. Discussion started: 26 September 2023

Figure 6. Restored seismic signal for the second debris flow in Fotangbagou gully. (a) Compensation function curve for monitoring station 1; (b) Time domain signal at monitoring station 1; (c) Frequency domain signal at monitoring station 1; (d) Time-frequency domain energy spectrum for monitoring station 2; (e) Compensation function curve for monitoring station 2; (f) Time domain signal at monitoring station 1; (g) Frequency domain signal at monitoring station 2; (h) Time-frequency domain energy spectrum for monitoring station 2. The magenta dashed lines in (c) and (g) are envelopes that represent peak amplitudes after processing.

4.2 Reconstruction of the debris flow evolution process

Taking the second Fotangbagou Gully debris flow as an example, we try reconstructing the debris flow process using seismic signal analysis. We will use infrared imagery and grain size data to analyze the effectiveness of the debris flow evolution process. And then, we will reconstruct the other two debris flows.

4.2.1 Process reconstruction by seismic

To obtain the reflection of debris flow evolution on seismic signals, we first processed the seismic signals according to the process shown in Figure 2 and got the time- and time-frequency figures (Figure 7). We analyzed the characteristics of the time-domain amplitude curve, the average amplitude, and the time-frequency spectrum of vertical direction to reconstruct the debris flow process.

Seismic signals from the two monitoring points in the gully correspond well, but there are some differences (Figure 7). Monitoring point 1 records the debris flow outbreak time as 7:25, after which the signal amplitude and frequency range increased rapidly. Signal amplitude peaked at 7:42 and then decayed slowly; while the frequency bandwidth rapidly increased from 8 to 43 Hz after debris flow initiation, which was maintained until 8.45 after which it reduced to 22 Hz. The seismic data at monitoring point 2 generally follow point 1, with debris flow outbreak recorded at 7:26 and signal amplitude peaking at 7:45 and then slowly decreasing. However, the frequency

https://doi.org/10.5194/egusphere-2023-2015
Preprint. Discussion started: 26 September 2023

bandwidth differs a little, being concentrated in the 10–40 Hz range between 7:30–7:50.

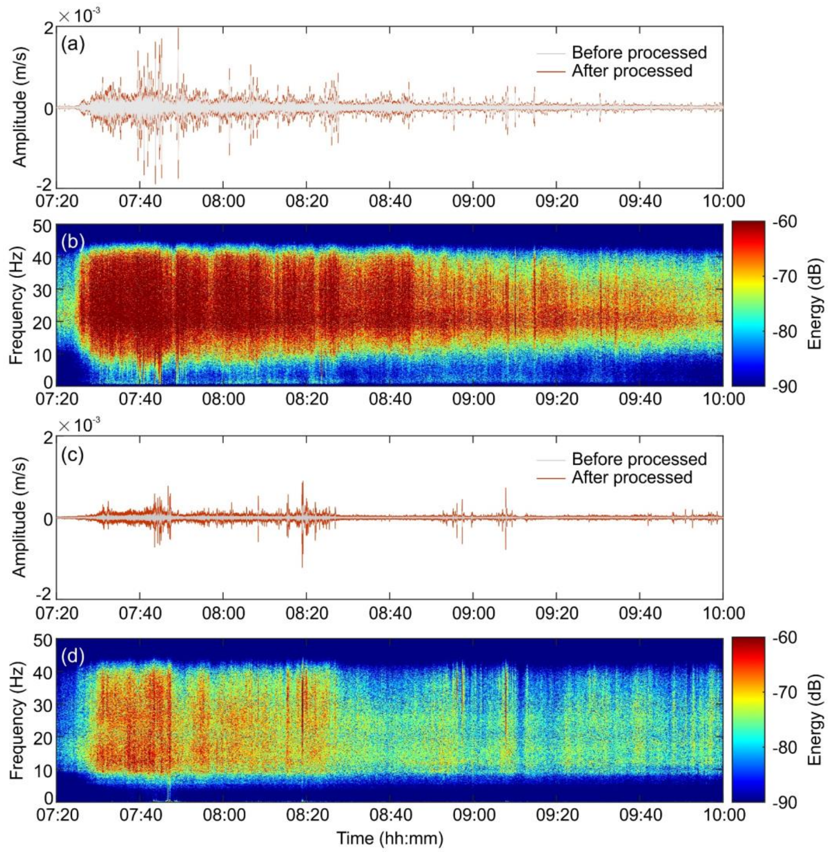

Figure 7. Restored seismic signal for the second debris flow in Fotangbagou gully. (a) Time domain signal at monitoring station 1; (b) Time-frequency domain energy spectrum for monitoring station 2; (c) Time domain signal at monitoring station 1; (d) Time-frequency domain energy spectrum for monitoring station 2.

The amplitude and frequency spectrum characteristics of the two stations are overall consistent but still have a certain difference. Comparing the seismic signal at the two monitoring points shows that monitoring point 1 recorded higher average amplitude, wider frequency bandwidth, and stronger energy time-frequency spectrum than monitoring point 2. However, the overall trend of the energy spectra, the absolute average amplitude, and the time domain amplitude are similar, showing a rapid rise and

https://doi.org/10.5194/egusphere-2023-2015
Preprint. Discussion started: 26 September 2023

a slow decline (Figure 7).

4.2.2 Infrared imagery analysis

Continuous infrared images record the development trend of debris flows that are reflected in seismic signals, so they can be used for verification. Infrared images taken at night have a small visible range and low resolution. The first Fotangba debris flow and the Ergou debris flow both occurred at night, making the low image quality unsuitable for our analysis. Therefore, infrared images for the second debris flow in Fotangba Gully, which occurred in the daytime, were used as an example for verification analysis.

Infrared images were obtained every 5 minutes from 7:39 to 8:04 (Figures 8a to 8f). Early infrared images (Figures 8a to 8d) show a gradual increase in flow rate, particle content, and flow velocity of the debris flow, peaking at 8:54, while later images (Figures 8d to 8f) show decreasing particle content and clear flow characteristics (Figure 8f). The overall trend shown by the seismic signal is consistent with this pattern, with energy peaking at about 7:40 and then slowly decreasing (Figure 6). From a macroscopic point of view, the seismic signal characterizes the debris flow development trend well. However, the timing of the peak state of the debris flow does not coincide with the infrared record. To help disentangle the reasons for the discrepancy, the dynamic features of the debris flow (flow rate, flow velocity, and particle content) reflected in the image are analyzed below.

At 7:39, the flow rate of the debris flow was still relatively low, and high point A in the old channel was not inundated (Figure 8a); the flow was in the channel to the right side of point A, and the flow rate in the left-hand channel was low, with no flooding or erosion of the left bank (point B). At 7:44, the debris flow began to flood point A and started to erode the left bank. Water depth and left bank erosion are at their maximum in the 7:59 image, after which water depth shallows. Overall, the infrared imagery shows a gradual increase in flow between 7:39–7:54 and a gradual decrease after 7:54. This appears to be supported by the presence of an eddy in the river channel near high

https://doi.org/10.5194/egusphere-2023-2015
Preprint. Discussion started: 26 September 2023

point A in Figures 8c and 8d, which is suggestive of high flow velocity. However, a more accurate picture of the flow velocity characteristics of the debris flow is obtained at point C (Figure 8a), located in the relatively smooth river channel. At point C, flow is most turbulent Figure 8a, indicating peak velocity, and then gradually decreases. Therefore, the infrared images show a decreasing trend in flow velocity after 7:39, which better matches the seismic record.

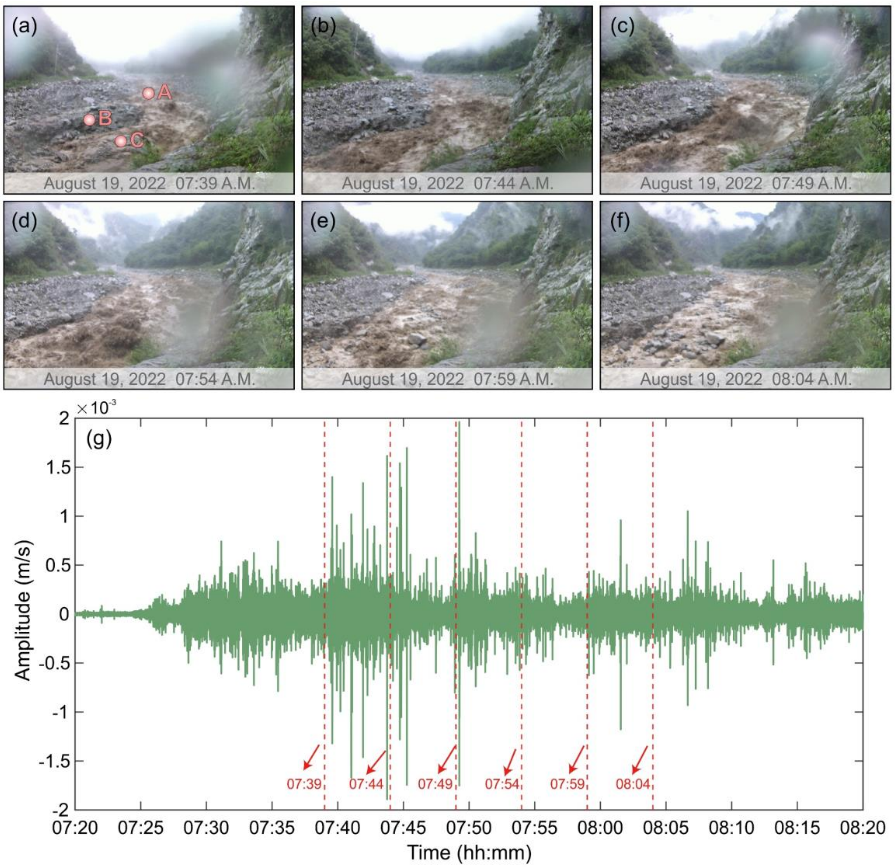

Figure 8. Infrared camera images and seismic signals were recorded at monitoring point 1 in Fotangbagou Gully during the second debris flow on the morning of August 19, 2022. Images were recorded every 5 minutes from 7:39 to 8:04: (a) 7:39 frame; (b) 7:44 frame; (c) 7:49 frame; (d) 7:54 frame; (e) 7:59 frame; (f) 8:04 frame. (g) The seismic signal was recorded at the point.

https://doi.org/10.5194/egusphere-2023-2015
Preprint. Discussion started: 26 September 2023

The infrared images show a gradual increase in the particle content of the debris flow from 7:39 to 7:49, with high particle content maintained between 7: 49 and 7:54 but far lower concentrations at 7:59 and 8:04. The debris flow evolution analysis showed flow velocity increased gradually from 7:39 to 7:59, and was relatively high; in this condition, there is intense erosion of accumulations next to the channel and entrainment along the flow path, which increases the proportion of solid phase in the fluid. As flow velocity decreases, erosion weakens and the particle content gradually decreases, turning the debris flow into a water flood. The presence of a rock at point A in Figures 8e and 8f illustrates the lack of transport capacity at this stage of the debris flow.

4.2.3 Post-event field investigation

The field investigation and UAV survey at Fotangbagou Gully started on the third day after the debris flow events, and nearby villagers confirmed the accumulation fans had not been disturbed. UAV aerial imagery of the accumulation fan at the gully mouth and close-ups of surface conditions are shown in Figures 9a–9c. Field measurements indicate the fan is about 1.2 m thick at Point C, with a thin layer (1–2 mm) of cohesive particles covering the surface in several areas (Figure 9c). Some huge rocks in Figures 9b and 9c show that the debris flow has a relatively high carrying capacity, and the rocks at the bottom of the alluvial fan are relatively large (Figure 9b), while the rocks in the front part of the alluvial fan (Figure 9c) are relatively small, indicating that the carrying capacity of the debris flow sharply decreases after it is released from the channel constraints (or in other words, the cross-sectional area increases).

A sediment sample was collected from the accumulation fans in the Fotangbagou gully to estimate the particle size distribution of the debris flow. The sample(Figure 9e) of about 4.7 kg was taken around the location marked ① in Figure 9a. Grain size analysis was undertaken by sieving and a Malvern particle sizer. The results show that cohesive particles, i.e., particles with grain size less than 0.005 mm, accounted for only

https://doi.org/10.5194/egusphere-2023-2015
Preprint. Discussion started: 26 September 2023

0.041% of the total weight of the sample from the channel (Figure 9d), which is consistent with field observations. The low cohesive sediment content could be due to removal by post-event processes, either by the flushing action of the Minjiang River or by human clearance of the impoundment fan. The particle size distribution shows that 94% of the particle size of this debris flow is 0.018 m, i.e., D in Equation (8). In the next section, we will use D as a guide for forward analysis of the PSD curve features of the debris flow.

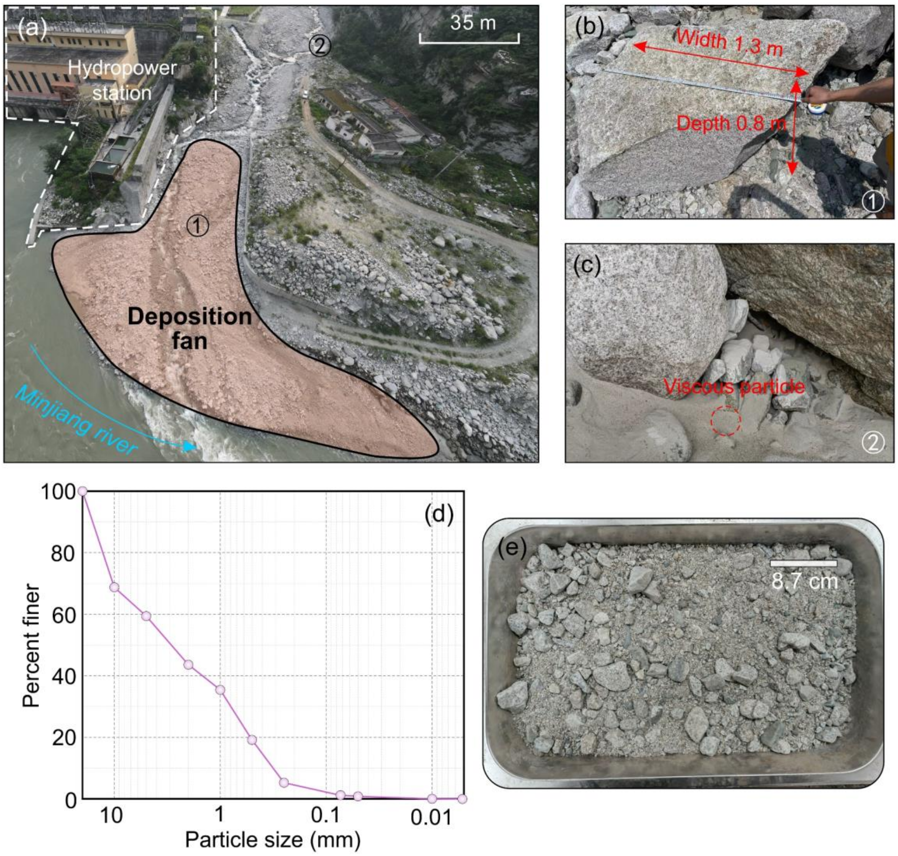

Figure 9. Post-event field survey of accumulation fans in Fotangbagou Gully. (a) Aerial view of the Fotangbagou gully fan; (b) Largest particle on the Fotangbagou gully fan, marked ① in image (a); (c) Thin layer of cohesive particles covering the accumulation surface in Fotangbagou gully, marked as ② in image (a); (d) Particle size distribution

https://doi.org/10.5194/egusphere-2023-2015
Preprint. Discussion started: 26 September 2023

for Fotangbagou gully sediment samples; (e) Fotangbagou gully sediment sample.

4.2.4 Key points analysis of PSD

Equation (7) was used to calculate the seismic PSD curves for the six-time points for which infrared images were obtained (Figure 10). Maximum energy shows a gradually decreasing trend from 7:39 to 8:04, while spectrum width first increases and then decreases. The high-frequency band gradually decreases from 7:39 to 8:04, but the high-frequency end, low-frequency end, and the maximum value of the energy frequency (peak frequency) show different trends. From 7:39 to 7:49, the high-frequency band decreases relatively quickly, and from 7:54 to 8:04, the speed and volume decrease slowly; at the low-frequency end, the energy of 7:44 is relatively large compared with the low-frequency end of 7:39 and 7:54 to 8:04. The energy change at the low-frequency end is relatively small; the maximum energy frequency change shows the characteristics of first increasing and then decreasing.

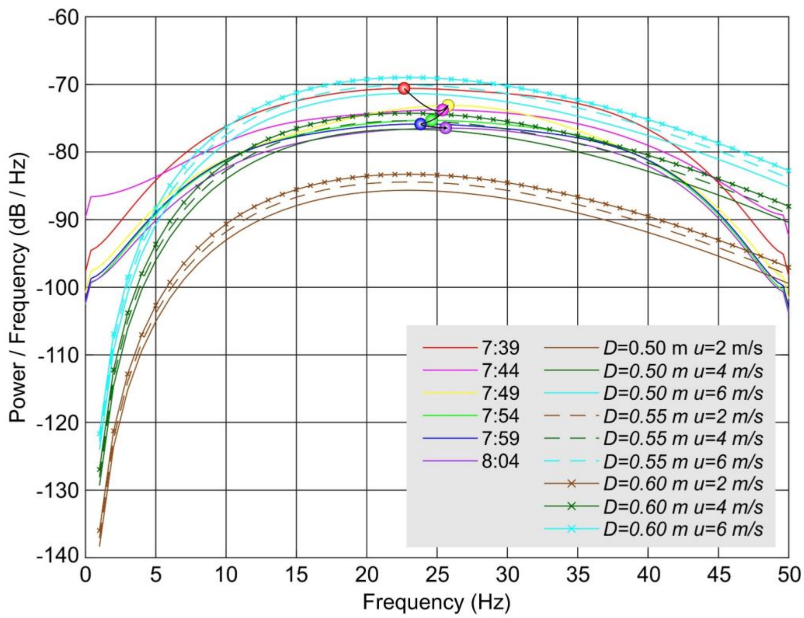

Figure 10. Evolution of power spectral density (PSD) during the second debris flow in Fotangbagou Gully on the morning of August 19, 2022, from 7:39 to 8:04 and

https://doi.org/10.5194/egusphere-2023-2015
Preprint. Discussion started: 26 September 2023

Comparison of power spectral density (PSD) for different grain sizes (*D*) and velocities (*u*). Each curve represents PSD frequency over 60 s. The six dots in the figure correspond to the PSD maximum at the six-time points from 7:39 to 8:04, and the black arrows indicate the time course of these six-time points.

To relate changes in frequency characteristics to the dynamic parameters of the debris flow, we performed a simple estimation of the PSD of the debris flow using Equation (8). The most important parameters are derived from the second debris flow in Fotangba. *D* in Equation (8) is based on 94% of the particle size of 0.018 m in the debris flow survey, which gives 0.5, 0.55, and 0.6 m. For flow velocity, maximum flow velocity values of 2, 4, and 6 m/s were used. Values for other parameters were those used for seismic signal recovery.

According to Figure 10, when D=0.5~0.6 m, u=4~6 m/s, the PSD of 10~40 Hz between 7:39 and 8:04 is approximately in this range. Compared with the result of 0.018 m in Figure 9(d), the particle size range D=0.5~0.6 m is 2~3 times larger than that of 0.018 m. This may be due to the intentional removal of larger particles during sampling, resulting in the collected soil samples having a small particle size during post-disaster investigations.

The forward modeling results about *D* and *u* (Figure 10) show that the velocity of the debris flow determines the energy level of the PSD, with particle size having a weaker effect on the energy than flow velocity. For the same particle radius, the energy of each frequency band increases sharply with flow velocity, while the increase in energy of each frequency band is relatively small with particle size for the same flow velocity. The influence of flow velocity is greater at the high-frequency end than at the low-frequency end; this means that changes in flow velocity can be determined using energy at the high-frequency end. For the six time points of the infrared images, the high-frequency end of the PSD curve shows a gradual decrease, indicating a gradual decrease in the debris flow velocity. The decrease is relatively rapid from 7: 39 to 7:59

https://doi.org/10.5194/egusphere-2023-2015
Preprint. Discussion started: 26 September 2023

and then slows, which supports the flow rate inferences from the infrared image analysis.

For the low-frequency band, the effect of velocity on energy is also relatively strong; as velocity decreases, the energy corresponding to a single frequency also decreases, but amplitude is relatively small compared to the high-frequency end in six frames (as shown in Figure 10). There is a tendency for a marked increase in the low-frequency end at 7:44 compared to 7:39, which is inconsistent with the analysis of the high-frequency end. The infrared image in Figure 8b shows a relatively high concentration of particles in the debris flow around 7:44, which may be responsible for the strong energy at the low-frequency end in this region.

Peak frequency is related to particle size and flow velocity. From Figure 10 about D and u, peak frequency is larger when the particle size is small, and the flow velocity is high than vice versa, which is due to the combined effect of particle size and flow velocity; at the same time, the particle content (flow and concentration) is one of the factors affecting the energy of seismic signals. The influence of particle concentration on the model shown in Equation (8) must be considered. The peak frequency of the debris flows seismic signal from 7:39 to 8:04 shown in Figure 10 first increases and then decreases and increases finally; from the comprehensive response of particle size and flow velocity to PSD, as the flow velocity decreases, the particle size of debris transported by the debris flow increases. A large change in flow velocity should be accompanied by changes in sediment concentration.

Based on our analysis, we infer that during the six moments from 7:39 to 8:04, flow velocity gradually decreases, and particle size, particle concentration, and flow velocity first increase and then decrease. This pattern is consistent with the results of infrared image analysis in Section 4.2.2 and verifies that debris flow trend can be determined from the time-frequency characteristics of seismic signals.

4.2.5 Reconstruction of 1st Fotangbagou and Ergou debris flow process

The seismic signal restoration was then completed using the same parameter

https://doi.org/10.5194/egusphere-2023-2015
Preprint. Discussion started: 26 September 2023

values as the first debris flow in section 4.1 for the first Fotangbagou debris flow. The horizontal distances between the channel and monitoring points 1 and 2 are 13 m and 7 m for Ergou Gully. For the Ergou debris flow restoration, a gain factor of 1.8 was used at monitoring station 1, and the parameter values for monitoring stations 2 and 1 of Fotangbagou were used for Ergou monitoring stations 1 and 2.

Seismic signal data for monitoring points 1 and 2 in Fontangbagou Gully are shown in Figures 11a to 11d. The first debris flow passed monitoring point 1 at about 3:07, after which debris flow movement gradually strengthened until 3:13 when the signal amplitude peaked and slowly declined thereafter. After the debris flow passed monitoring point 2 around 3:10, there were about 120 s of rapid vibration, amplitude peaked, then the seismic signal began to weaken. After about 160 s, debris flow movement gradually strengthened to a second amplitude peak at 3:24 and then decayed slowly. The seismic signal was stronger at monitoring point 1 than at point 2, and there was a general decrease in energy generated by the movement of the debris flow between the two points. The time-frequency characteristics of the seismic signal at monitoring point 1 (Figure 11b) show energy is concentrated in the 12–44 Hz range between 3:07–4:25, and over the entire event, energy decays toward 21 Hz. At monitoring point 2 (Figure 11d), energy is concentrated in the 10–42 Hz range between 3:10–4:00, and over the entire event, energy decays toward 21 Hz. At both monitoring points, the energy spectra show the same pattern of rapid rise and slow decline of the amplitude seismic signal in the time domain.

https://doi.org/10.5194/egusphere-2023-2015
Preprint. Discussion started: 26 September 2023

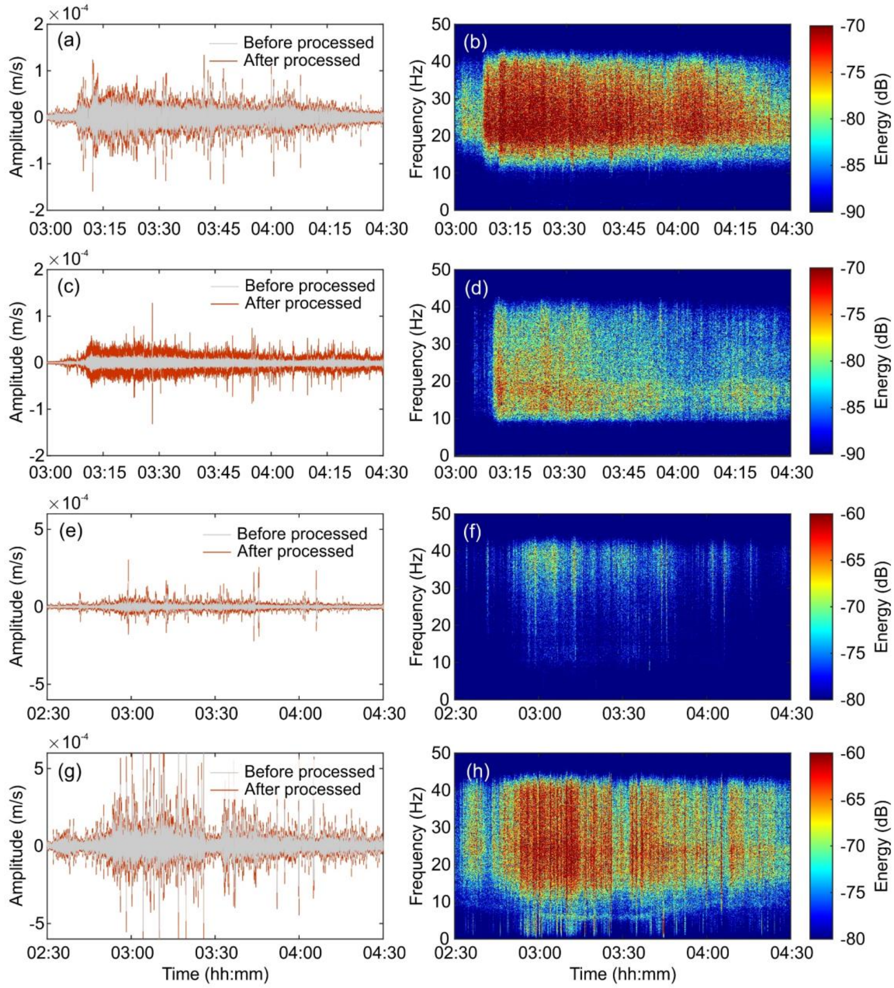

Figure 11. seismic and its time-frequency spectrum of the first debris flow in Fotangbagou gully and debris flow in Ergou gully. The first Fotangbagou debris flow's Seismic recorded at monitoring stations 1 (a) and station 2 (c), and (b) and (d) is its time-frequency spectrum respectively; The Ergou debris flow's Seismic recorded at monitoring station 1 (e) and station 2 (g), and (f) and (h) is its time-frequency spectrum respectively.

Seismic signal data for the two monitoring points in Ergou Gully are shown in Figures 11e to 11h. As the debris flow passed monitoring point 1 at about 2:38, it was

https://doi.org/10.5194/egusphere-2023-2015
Preprint. Discussion started: 26 September 2023

moving rapidly and strongly; signal amplitude peaked at 2:56 and then decayed slowly. The debris flow passed monitoring point 2 at about 2:44, with signal amplitude peaking at 2:58 and slowly decaying. In contrast to Fotangbagou Gully, the seismic signal was stronger at monitoring point 2 than at monitoring point 1, and the energy generated by the movement of the debris flow increased between the two monitoring points. The time-frequency characteristics of the seismic signal at monitoring point 1 show energy is concentrated in the 30–40 Hz range between 2:50–4:00 (Figure 11f). At monitoring point 2, energy is concentrated in the 6–45 Hz range between 2:45–4:30 (Figure 11h). Over the entire event, energy decays toward 23 Hz. As with the Fontangbagou debris flow, the overall trend of the energy spectra is consistent with the amplitude range in the time domain, with a rapid rise and a slow decline.

4.3 Debris flow scale analysis by seismic signal

We use the frequency and amplitude parameters of the original signal to analyze the relative scale of the three debris flows. Due to the different types of sensors used in Fotangbagou and Ergou, there is a gap between the instrument response. When comparing the scale between debris flows, we will use frequency width and main frequency for comparison. When the flow velocity and discharge are analyzed for different monitoring stations, the comparison of the amplitude will be increased. The relative scale of the Ergou and Fotangbagou debris flows can be verified by information such as the amount of accumulation material, particle size, and the maximum stone of the post-event survey.

Section 4.2.5 showed the decay of the seismic signals differed between monitoring stations, so to improve the debris flow scale analysis, the seismic signals that decayed during propagation need to be restored; this was done using Equations (9) and (10). From the restored original seismic signal, the maximum amplitudes and bandwidths can be used to assess the relative magnitudes of the three debris flows. The maximum amplitudes of the frequency domain spectrum for the first and second Fotangbagou debris flows, and the Ergou debris flow are 0.0045, 0.02, and 0.012, respectively, and

https://doi.org/10.5194/egusphere-2023-2015
Preprint. Discussion started: 26 September 2023

bandwidths are 11.64, 41.12, and 27.36 Hz, respectively. Therefore, the first and second Fotangbagou debris flows are large- and small-scale events and the Ergou debris flow is medium-scale.

4.4 Debris flow velocity analysis

The time domain signal was used to solve the maximum velocity of each debris flow between the two monitoring stations using the cross-correlation algorithm (Equation 4). The velocity result for Ergou gully is an order of magnitude higher than for Fotangbagou gully and is outside the normal debris flow range (Table 3). The signal lag time τ reflected by the peak amplitude of the second debris flow in Fontangbagou gully is 74 s (Figure 12), and the distance between adjacent monitoring sections is about 520 m, which gives a peak velocity of 7.027 m/s (Table 3).

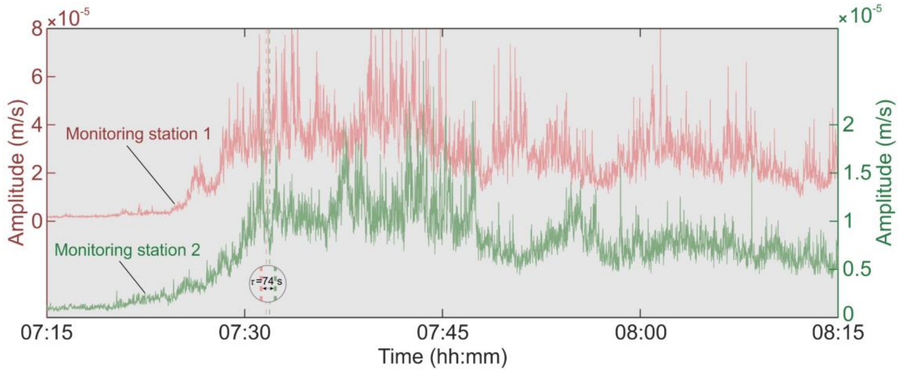

Figure 12. Amplitude range (vertical direction) of the second debris flow in Fotangbagou gully based on the cross-correlation algorithm. The signal lag time τ between the two monitoring stations is circled.

Table 3 Results of maximum velocity calculations for Fotangbagou gully and Ergou gully debris flows.

Debris flow	Maximum velocity calculated using each method (m/s)	
	Cross-correlation algorithm	Manning formula
First debris flow in Fotangbagou Gully	3.006	—
Second debris flow in	7.027	7.921

https://doi.org/10.5194/egusphere-2023-2015
Preprint. Discussion started: 26 September 2023

Fotangbagou Gully Debris flow in Ergou Gully	38.333	—

To verify the reliability of the velocity calculations based on the cross-correlation algorithm, peak velocity was also determined using the Manning formula (Equation 5). Channel parameters were extracted from cross-sections at the monitoring stations (Figure 13). A key element of the Manning method is the channel roughness coefficient *n* (Equation 8), which was determined as 0.05 for the Fotangbagou gully. Previous work by Guo et al. (2016) obtained an *n* value of 0.1 for a debris flow in the Ergou Gully in 2013. Since the terrain of Fotangbagou Gully is less rugged than that of Ergou Gully, the calculated *n* value of 0.05 is reasonable. The gradient ratio *J* of the monitoring section was determined using the digital surface model (DSM) output of the UAV aerial survey. The hydraulic radius *R* is obtained by dividing the area of the monitoring section (based on the DSM) by the wet perimeter. The wet perimeter can be used to estimate the depth of debris flow based on the infrared camera monitoring picture, and further combined with the monitoring section to determine the wet perimeter. However, since the nighttime infrared images could not be used, *R* could only be determined for the second debris flow in the Fotangbagou gully, which took place in daylight. Using the Manning formula on this event, the maximum debris flow velocity at monitoring points 1 and 2 was calculated as 7.817 and 7.921 m/s, respectively. Taking the larger figure, this indicates the calculation error of the cross-correlation algorithm is 11.29%.

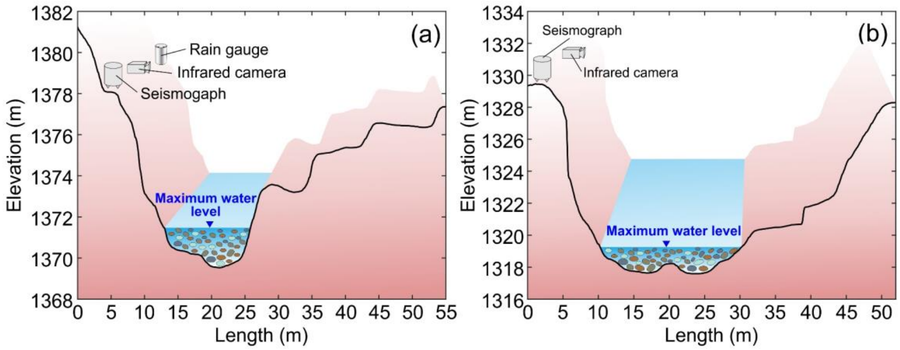

https://doi.org/10.5194/egusphere-2023-2015
Preprint. Discussion started: 26 September 2023

Figure 13. Cross-sections of Fotangbagou gully showing maximum water level used in calculation of peak velocity by the Manning formula. (a) Monitoring station 1; (b) Monitoring station 2.

5 Discussion

5.1 Characteristics and evolution of debris flow events

The time- and time-frequency domain characteristics of the seismic signal showed similar patterns of a rapid initial rise followed by a slow decline for all three debris flows (Figures 7 and 11). Due to the absorption and attenuation of seismic waves by the surface, the range of seismic signals from debris flows recorded by the monitoring system near the channel is relatively large. For example, the time-frequency spectrum of the seismic signal recorded at most monitoring points of the three debris flows in this study is significant, as shown in Figures 7b, 11b, 11d, and 11h, but unlike Figures 7d and 11f, the energy decreases toward 20 to 23 Hz throughout the event. But all stations also have common time-frequency spectrum properties. The time-frequency spectrum properties of all signals are high-energy and are mainly in the frequency range of 10 to 42 Hz. Therefore, when using seismic debris flow signals for debris flow analysis, it is necessary to recover their energy.

For the same debris flow, the kinematic parameters such as flow velocity, particle diameter distribution, concentration, flow rate, etc., vary with the topography (Figure 13) and the distance of the seismic signal from the sensor, so the signal amplitude recorded at each monitoring point is different. The change in time domain signal can roughly reflect the debris flow evolution characteristics, but the analysis of flow velocity, concentration, and flow of the debris flow must be combined with the change characteristics of the PSD curve for a comprehensive analysis; the debris flow must be fully considered when selecting the PSD curve analysis time. Seismic features select representative analysis points. Second, when analyzing the characteristics of PSD curve changes, it is best to estimate the approximate flow velocity and particle size of the

https://doi.org/10.5194/egusphere-2023-2015
Preprint. Discussion started: 26 September 2023

debris flow, as the flow velocity and particle size change by orders of magnitude, the characteristics of the PSD curve, typically the flow velocity and the degree of influence of particle size change even more. Thus, when seismic signals are used for debris-flow evolution analysis, sufficient information on the post-disaster investigation and dynamic parameters of the debris flow, combined with the forward modeling results for the joint analysis, increase the reliability of the analysis results.

5.2 Velocity and scale of debris flow

Comparing the maximum velocity calculations from the cross-correlation algorithm and Manning's formula suggested an error of around 11% for the cross-correlation results of the Fotangbagou gully debris flows (Table 3). Comiti et al. (2014) suggested that the cross-correlation algorithm tends to underestimate debris flow velocity, which is the case here. A factor that might influence the velocity calculation based on the cross-correlation algorithm is the distance between seismic sensors. The sensors deployed in this study are about 500 m apart, and Arattano and Marchi (2005) suggested that spacing of 100+ m may reduce the accuracy of debris flow velocity calculation based on the cross-correlation algorithm. Also, the empirical nature of the Manning formula versus the cross-correlation algorithm might lead to differences in the velocity results of the two methods (Kang, 1987).

For the Ergou gully debris flow, the cross-correlation velocity result is an order of magnitude too large. This discrepancy may be due to the nature of the velocity calculation method or factors related to local field conditions. The anomalous result for Ergou Gully may be due to the winding and narrow gully topography; a tight bend between the two monitoring stations means that the kinematic parameters of the debris flow change markedly along the course, which may confound velocity calculations. Several studies have shown that debris flow characteristics are strongly influenced by gully topography and monitoring section characteristics (Huang et al., 2007; Cucchiaro et al., 2018). Differences in the kinematic parameters of the debris flows may explain the discrepancy in cross-correlation algorithm results (Table 3); calculation of peak

https://doi.org/10.5194/egusphere-2023-2015
Preprint. Discussion started: 26 September 2023

velocity using the cross-correlation algorithm might only apply to some debris flows.

The applicability of the cross-correlation algorithm for peak velocity calculation in different topographic settings would be a good focus for future research. However, provided there are no (topographic or other) factors affecting the seismic signal generated by the evolution of the debris flow, the average velocity calculation from the cross-correlation algorithm is considered reliable.

Two different types of seismic monitoring equipment were deployed in the gullies, seismographs in one and geophones in the other, which possibly explains the different parameter sets in section 4.4. Furthermore, some parameters are estimated experientially, such as Rayleigh wave velocity in channels with gravel. These factors may affect debris flow scale analysis.

5.3 Limitations and future works

There were some issues with the application of infrared cameras in the study. The cameras were not able to record images of nighttime debris flows. Even for daytime debris flows, factors such as rainfall or debris flow splashes caused water droplets to adhere to the infrared camera lens, partially blurring the recorded images. Also, the 5-minute interval between recorded images is fine for determining debris flow movement, but the time resolution is too coarse to determine changes in flow characteristics during debris flow evolution. In follow-up studies, the interval between images should be increased. It would also be useful to have a wider array of instruments at each monitoring station, including flow level gauges, to aid seismic signal analysis and velocity estimation and emplace more stations over a larger area to generate a larger dataset. This would allow future research to focus on the identification of early warning thresholds for debris flow disasters.

The small dataset of the current study does not allow a broader analysis of debris flow dynamics; however, it does demonstrate the effectiveness of using an in-situ seismic network for real-time monitoring of debris flows, provides theoretical support for the inversion of debris flow dynamics, and highlights the potential for application

https://doi.org/10.5194/egusphere-2023-2015
Preprint. Discussion started: 26 September 2023

in early warning systems.

6 Conclusions

In this study, the characteristics of the seismic signal from three debris flows on August 19, 2022, in the Wenchuan earthquake area of China are investigated. The three debris flow events studied here were generated under conditions of heavy rainfall. Both the time- and frequency domain characteristics of the seismic signal follow the same pattern of a rapid rise and slow decay, which shows that debris flow outbreaks rapidly and retreats slowly and causes the hazard duration for a long time. Even to a large extent eliminating the propagation effect, the seismic amplitude and frequency characteristics of different monitoring stations have a large difference, which indicates that the dynamic parameters of the debris flow are changing in the evolution process. The change in the flow state of the debris flow results in a different range of frequencies in the energy spectrum at the beginning and end of the debris flow, which is confirmed by our continuous photo analysis, PSD of the current records, and PSD of the forward modeling. At the start of the debris flow, the energy is strong when debris flow goes through the monitoring point, mainly in the 10–42 Hz frequency range, while later in the event, energy is in the 20–23 Hz frequency range. According to the seismic amplitude and frequency characteristic changes at different monitoring points of debris flows, the relative changes in the debris flow evolution process can be roughly analyzed. Through differences in different debris flow frequency characteristics, the relative scale between the two debris flows can be qualitatively analyzed.

The cross-correlation algorithm can be a good choice to calculate maximum debris flow velocity in relative debris flow with riverbed changing simply, the second debris flow in Fotangbagou gully calculated out the max velocity is 7.027 m/s proven to be reasonable by the Manning formula. However, in Ergou Gully with relatively complex topography, the cross-correlation algorithm was less successful, probably due to its more complex topographic setting causing strong variations in the kinematic parameters of the debris flow. Hence, the cross-correlation algorithm may be an appropriate approach for peak flow calculation in simple debris flow, but not appropriate in much more complex debris flow.

Acknowledgments

This study was financially supported by the National Natural Science Foundation of China (grant nos. U21A2008, 42120104002, and 42271075), the Second Tibetan Plateau Scientific Expedition and Research Program (STEP) (grant no. 2019QZKK0906).

Code/Data availability

All raw data can be provided by the corresponding authors upon request.

Author contributions

The authors of this manuscript entitled "Real-time Monitoring and Analysis of Debris Flow Events: Insight from seismic signal features and dynamic flow characteristics" are Yan Yan, Cheng Zeng, Yifei Cui, Sheng Hu, Xinglu Wang, and Hui Tang. Yan Yan is the first author, is responsible for Conceptualization, Methodology, Writing- Original draft preparation in this research. Cheng Zeng is the second author, is responsible for the Software, Data curation, Validation, Writing-Original draft preparation. Yifei Cui is the third author and the corresponding author, is responsible for the Review & Editing, Supervision. Sheng Hu is the fourth author and is responsible for Visualization. Xinglu Wang is responsible for the Investigation, Validation. Hui Tang is the sixth author and is responsible for Writing- Reviewing and Editing.

Competing interests

The authors declare that they have no conflict of interest.

https://doi.org/10.5194/egusphere-2023-2015
Preprint. Discussion started: 26 September 2023

References

Allstadt, K.E., Farin, M., Lockhart, A.B., McBride, S.K., Kean, J.W., Iverson, R.M., Logan, M., Smith, J.B., Tsai, V.C., George, D., 2019. Overcoming barriers to progress in seismic monitoring and characterization of debris flows and lahars. Association of Environmental and Engineering Geologists, Special Publication 28.

Andrade, S.D., Almeida, S., Saltos, E., Pacheco, D., Hernandez, S., Acero, W., 2022. A simple and general methodology to calibrate seismic instruments for debris flow quantification: application to Cotopaxi and Tungurahua volcanoes (Ecuador). Landslides 19(3), 747-759.

Arattano, M., 1999. On the use of seismic detectors as monitoring and warning systems for debris flows. Nat. Hazards 20(2-3), 197-213.

Arattano, M., Cavalli, M., Comiti, F., Coviello, V., Macconi, P., Marchi, L., 2015. Standardization of methods and procedures for debris flow seismic monitoring. In: Lollino, G., Arattano, M., Rinaldi, M., Giustolisi, O., Marechal., J.-C., Grant, G.E. (Eds.), Engineering Geology for Society and Territory-Volume 3: River Basins, Reservoir Sedimentation and Water Resources. Springer International Publishing, Switzerland, pp. 63-67.

Arattano, M., Marchi, L., 2005. Measurements of debris flow velocity through cross-correlation of instrumentation data. Nat. Hazards Earth Syst. Sci. 5(1), 137-142.

Arattano, M., Marchi, L., 2008. Systems and sensors for debris-flow monitoring and warning. Sensors 8(4), 2436-2452.

Arattano, M., Moia, F.,1999. Monitoring the propagation of a debris flow along a torrent. Hydrol. Sci. J. 44(5), 811-823.

Barrière, J., Oth, A., Hostache, R., Krein, A., 2015. Bed load transport monitoring using seismic observations in a low-gradient rural gravel bed stream. Geophys. Res. Lett. 42(7), 2294-2301.

Beason, S.R., Legg, N.T., Kenyon, T.R., Jost, R.P., 2021. Forecasting and seismic detection of proglacial debris flows at Mount Rainier National Park, Washington, USA. Environ. Eng. Geosci. 27(1), 57-72.

Berti, M., Genevois, R., LaHusen, R., Simoni, A., Tecca, P.R., 2000. Debris flow monitoring in the Acquabona watershed on the Dolomites (Italian Alps). Physics and Chemistry of the Earth, Part B: Hydrology, Oceans and Atmosphere 25(9), 707-715.

Bessason, B., Eiríksson, G., Thorarinsson, Ó., Thórarinsson, A., Einarsson, S., 2007. Automatic detection of avalanches and debris flows by seismic methods. J. Glaciol. 53(182), 461-472.

Burtin, A., Bollinger, L., Cattin, R., Vergne, J., Nábělek, J.L., 2009. Spatiotemporal sequence of Himalayan debris flow from analysis of high-frequency seismic noise. J. Geophys. Res. 114, F04009.

Cao, C., Yu, B., Ma, E.L., Liu, S., 2019. Study on debris flow in Fongtuba Gully after the earthquake at Wenchuan County of Sichuan Province. Journal of Sediment Research 44(1), 38-43 (in Chinese).

Chen, C.Y., Lin, L.Y., Yu, F.C., Lee, C.S., Tseng, C.C., Wang, A.H., Cheung, K.W., 2007. Improving debris flow monitoring in Taiwan by using high-resolution rainfall products from QPESUMS.

https://doi.org/10.5194/egusphere-2023-2015
Preprint. Discussion started: 26 September 2023

Nat. Hazards 40, 447-461.

Chien-Yuan, C., Tien-Chien, C., Fan-Chieh, Y., Wen-Hui, Y., Chun-Chieh, T., 2005. Rainfall duration and debris-flow initiated studies for real-time monitoring. Environ. Geol. 47, 715-724.

Comiti, F., Marchi, L., Macconi, P., Arattano, M., Bertoldi, G., Borga, M., Brardinoni, F., Cavalli, M., D'Agostino, V., Pennna, D., Theule, J., 2014. A new monitoring station for debris flows in the European Alps: first observations in the Gadria basin. Nat. Hazards 73, 1175-1198.

Cook, K. L., Dietze, M., 2022. Seismic advances in process geomorphology. Annu. Rev. Earth Planet. Sci. 50, 183-204.

Coviello, V., Arattano, M., Turconi, L., 2015. Detecting torrential processes from a distance with a seismic monitoring network. Nat. Hazards 78, 2055-2080.

Cucchiaro, S., Cavalli, M., Vericat, D., Crema, S., Llena, M., Beinat, A., Marchi, L., Cazorzi, F., 2018. Monitoring topographic changes through 4D-structure-from-motion photogrammetry: application to a debris-flow channel. Environ. Earth Sci. 77, 1-21.

Cui, P., Guo, X., Yan, Y., Li, Y., Ge, Y., 2018. Real-time observation of an active debris flow watershed in the Wenchuan Earthquake area. Geomorphology 321, 153-166.

Cui, P., Zhou, G.G., Zhu, X.H., Zhang, J.Q., 2013. Scale amplification of natural debris flows caused by cascading landslide dam failures. Geomorphology 182, 173-189.

Dammeier, F., Moore, J.R., Hammer, C., Haslinger, F., Loew, S., 2016. Automatic detection of alpine rockslides in continuous seismic data using hidden Markov models. J. Geophys. Res. 121(2), 351-371.

Deparis, J., Jongmans, D., Cotton, F., Baillet, L., Thouvenot, F., Hantz, D., 2008. Analysis of rock-fall and rock-fall avalanche seismograms in the French Alps. Bull. Seismol. Soc. Amer. 98(4), 1781-1796.

Ekström, G., Stark, C.P., 2013. Simple scaling of catastrophic landslide dynamics. Science 339(6126), 1416-1419.

Fuchs, F., Lenhardt, W., Bokelmann, G., AlpArray Working Group, 2018. Seismic detection of rockslides at regional scale: examples from the Eastern Alps and feasibility of kurtosis-based event location. Earth Surf. Dyn. 6(4), 955-970.

Guo, X., Cui, P., Li, Y., Zou, Q., Kong, Y., 2016. The formation and development of debris flows in large watersheds after the 2008 Wenchuan Earthquake. Landslides 13, 25-37.

Hibert, C., Mangeney, A., Grandjean, G., Shapiro, N.M., 2011. Slope instabilities in Dolomieu crater, Réunion Island: From seismic signals to rockfall characteristics. J. Geophys. Res. 116, F04032.

Huang, C.J., Yin, H.Y., Chen, C.Y., Yeh, C.H., Wang, C.L., 2007. Ground vibrations produced by rock motions and debris flows. J. Geophys. Res. 112, F02014.

Huang, X., Li, Z., Fan, J., Yu, D., Xu, Q., 2020. Frequency characteristics and numerical computation of seismic records generated by a giant debris flow in Zhouqu, Western China. Pure Appl. Geophys. 177, 347-358.

Hübl, J., Schimmel, A., Kogelnig, A., Suriñach, E., Vilajosana, I., McArdell, B.W., 2013. A review on acoustic monitoring of debris flow. International Journal of Safety and Security Engineering 3(2), 105-115.

Hürlimann, M., Abancó, C., Moya, J., Vilajosana, I., 2014. Results and experiences gathered at the

https://doi.org/10.5194/egusphere-2023-2015
Preprint. Discussion started: 26 September 2023

Rebaixader debris-flow monitoring site, Central Pyrenees, Spain. Landslides 11, 939-953.

Hürlimann, M., Coviello, V., Bel, C., Guo, X., Berti, M., Graf, C., Hürl, J., Miyata, S., Smith, J.B., Yin, H.-Y., 2019. Debris-flow monitoring and warning: Review and examples. Earth-Sci. Rev. 199, 102981.

Hürlimann, M., Rickenmann, D., Graf, C., 2003. Field and monitoring data of debris-flow events in the Swiss Alps. Can. Geotech. J. 40(1), 161-175.

Iverson, R.M., 1997. The physics of debris flows. Rev. Geophys. 35(3), 245-296.

Kang, Z.C., 1987. A velocity research of debris flow and its calculating method in China. Mountain Research 5(4), 247-259.

Kean, J.W., Staley, D.M., Lancaster, J.T., Rengers, F.K., Swanson, B.J., Coe, J.A., Hernandez, J.L., Sigman, A.J., Allstadt, K.E., Lindsay, D.N., 2019. Inundation, flow dynamics, and damage in the 9 January 2018 Montecito debris-flow event, California, USA: Opportunities and challenges for post-wildfire risk assessment. Geosphere 15(4), 1140-1163.

Kjartansson, E., 1979. Constant Q - wave propagation and attenuation. J. Geophys. Res.-Solid Earth 84(B9), 4737-4748.

Kogelnig, A., Hübl, J., Suriñach, E., Vilajosana, I., McArdell, B.W., 2014. Infrasound produced by debris flow: propagation and frequency content evolution. Nat. Hazards 70, 1713-1733.

Lai, V.H., Tsai, V.C., Lamb, M.P., Ulizio, T.P., Beer, A.R., 2018. The seismic signature of debris flows: Flow mechanics and early warning at Montecito, California. Geophys. Res. Lett. 45(11), 5528-5535.

Li, C., Wang, X., He, C., Wu, X., Kong, Z., Li, X., 2019. China National Digital Geological Map (Public Version at 1:200 000 Scale) Spatial Database(V1). Development and Research Center of China Geological Survey; China Geological Survey[producer], 1957. National Geological Archives of China [distributor], 2019-06-30. 10.23650/data.A.2019.NGA120157.K1.1.1. V1; http://dcc.ngac.org.cn/geologicalData/rest/geologicalData/geologicalDataDetail/8adaeff96db9707f016dc819cb1f02c0

Li, Z., Huang, X., Xu, Q., Yu, D., Fan, J., Qiao, X., 2017. Dynamics of the Wulong landslide revealed by broadband seismic records. Earth, Planets and Space 69, 1-10.

Liu C., Feng X., Zhang J., 2013. A stable inverse Q filtering using the iterative filtering method. Oil Geophysical Prospecting 48(6), 890-895 (in Chinese).

Liu, S., Hu, K., Zhang, Q., Zhang, S., Hu, X., Tang, D., 2021. Quantitative analysis of the effects of an earthquake on rainfall thresholds for triggering debris-flow events. Front. Earth Sci. 9, 676470.

Marchetti, E., Walter, F., Barfucci, G., Genco, R., Wenner, M., Ripepe, M., McArdell, B., Price, C., 2019. Infrasound array analysis of debris flow activity and implication for early warning. J. Geophys. Res. 124(2), 567-587.

Marchi, L., Arattano, M., Deganutti, A.M., 2002. Ten years of debris-flow monitoring in the Moscardo Torrent (Italian Alps). Geomorphology 46(1-2), 1-17.

Moretti, L., Mangeney, A., Capdeville, Y., Stutzmann, E., Huggel, C., Schneider, D., Bouchut, F., 2012. Numerical modeling of the Mount Steller landslide flow history and of the generated long period seismic waves. Geophys. Res. Lett. 39(16), L16402.

Schimmel, A., Coviello, V., Comiti, F., 2022. Debris flow velocity and volume estimations based

https://doi.org/10.5194/egusphere-2023-2015
Preprint. Discussion started: 26 September 2023

on seismic data. Nat. Hazards Earth Syst. Sci. 22(6), 1955-1968.

Schimmel, A., Hübl, J., 2016. Automatic detection of debris flows and debris floods based on a combination of infrasound and seismic signals. Landslides 13, 1181-1196.

Schneider, D., Bartelt, P., Caplan‐Auerbach, J., Christen, M., Huggel, C., McArdell, B.W., 2010. Insights into rock-ice avalanche dynamics by combined analysis of seismic recordings and a numerical avalanche model. J. Geophys. Res. 115, F04026.

Smart, G.M., 1999. Coefficient of friction for flow resistance in alluvial channels. Proc. Inst. Civil Eng.-Water Marit. Energy 136(4), 205-210.

Suwa, H., Okano, K., Kanno, T., 2009. Behavior of debris flows monitored on test slopes of Kamikamihorizawa Creek, Mount Yakedake, Japan. International Journal of Erosion Control Engineering 2(2), 33-45.

Tang, C., Rengers, N.V., Van Asch, T.W., Yang, Y.H., Wang, G.F., 2011. Triggering conditions and depositional characteristics of a disastrous debris flow event in Zhouqu city, Gansu Province, northwestern China. Nat. Hazards Earth Syst. Sci. 11(11), 2903-2912.

Tecca, P.R., Galgaro, A., Genevois, R., Deganutti, A.M., 2003. Development of a remotely controlled debris flow monitoring system in the Dolomites (Acquabona, Italy). Hydrol. Process. 17(9), 1771-1784.

Tsai, V.C., Minchew, B., Lamb, M.P., Ampuero, J.P., 2012. A physical model for seismic noise generation from sediment transport in rivers. Geophys. Res. Lett. 39(2), L02404.

Van Herwijnen, A., Schweizer, J., 2011. Monitoring avalanche activity using a seismic sensor. Cold Reg. Sci. Tech. 69(2-3), 165-176.

Vilajosana, I., Suriñach, E., Abellán, A., Khazaradze, G., Garcia, D., Llosa, J., 2008. Rockfall induced seismic signals: case study in Montserrat, Catalonia. Nat. Hazards Earth Syst. Sci. 8(4), 805-812.

Walter, F., Burtin, A., McArdell, B.W., Hovius, N., Weder, B., Turowski, J.M., 2017. Testing seismic amplitude source location for fast debris-flow detection at Illgraben, Switzerland. Nat. Hazards Earth Syst. Sci. 17(6), 939-955.

Yan, Y., Cui, P., Chen, S., Chen, X., Chen, H., Chien, Y., 2017. Characteristics and interpretation of the seismic signal of a field-scale landslide dam failure experiment. J. Mt. Sci. 14, 219-236.

Yan, Y., Cui, Y., Huang, X., Zhou, J., Zhang, W., Yin, S., Guo, J., Hu, S., 2022. Combining seismic signal dynamic inversion and numerical modeling improves landslide process reconstruction. Earth Surf. Dynam. 10, 1233–1252.

Yan, Y., Cui, Y., Liu, D., Tang, H., Li, Y., Tian, X., Zhang, L., Hu, S., 2021. Seismic signal characteristics and interpretation of the 2020 “6.17” Danba landslide dam failure hazard chain process. Landslides 18, 2175-2192.

Yan, Y., Tang, H., Hu, K., Turowski, J. M., Wei, F., 2023. Deriving debris-flow dynamics from real-time impact-force measurements. J. Geophys. Res. 128, e2022JF006715.

Yan, Y., Cui, Y., Tian, X., Hu, S., Guo, J., Wang, Z., Yin S., Liao, L., 2020. Seismic signal recognition and interpretation of the 2019 “7.23” Shuicheng landslide by seismogram stations. Landslides 17, 1191-1206.

Yu, G., Lim, S.Y., 2003. Modified Manning formula for flow in alluvial channels with sand-beds. J. Hydraul. Res. 41(6), 597-608.